

Measurements of CP Violation in $B^0 \rightarrow D^{*-}\pi^+$ and $B^0 \rightarrow D^-\pi^+$ Decays

F. J. Ronga,⁷ T. R. Sarangi,⁷ K. Abe,⁷ I. Adachi,⁷ H. Aihara,⁴⁵ D. Anipko,¹ K. Arinstein,¹ Y. Asano,⁴⁹
 T. Aushev,¹¹ A. M. Bakich,⁴⁰ V. Balagura,¹¹ E. Barberio,¹⁹ M. Barbero,⁵ K. Belous,¹⁰ U. Bitenc,¹² I. Bizjak,¹²
 S. Blyth,²² A. Bondar,¹ A. Bozek,²⁵ M. Bračko,^{7,18,12} T. E. Browder,⁵ P. Chang,²⁴ A. Chen,²² W. T. Chen,²²
 B. G. Cheon,³ R. Chistov,¹¹ Y. Choi,³⁹ A. Chuvikov,³³ J. Dalseno,¹⁹ M. Danilov,¹¹ M. Dash,⁵⁰ A. Drutskoy,⁴
 S. Eidelman,¹ D. Epifanov,¹ S. Fratina,¹² N. Gabyshev,¹ A. Garmash,³³ T. Gershon,⁷ G. Gokhroo,⁴¹ B. Golob,^{17,12}
 A. Gorišek,¹² J. Haba,⁷ K. Hara,⁷ T. Hara,³⁰ K. Hayasaka,²⁰ H. Hayashii,²¹ M. Hazumi,⁷ T. Higuchi,⁷ L. Hinz,¹⁶
 T. Hokuue,²⁰ Y. Hoshi,⁴³ S. Hou,²² W.-S. Hou,²⁴ T. Iijima,²⁰ K. Inami,²⁰ A. Ishikawa,⁴⁵ H. Ishino,⁴⁶ R. Itoh,⁷
 Y. Iwasaki,⁷ J. H. Kang,⁵¹ H. Kawai,² T. Kawasaki,²⁷ H. R. Khan,⁴⁶ H. J. Kim,¹⁵ K. Kinoshita,⁴ S. Korpar,^{18,12}
 P. Krokovny,¹ R. Kulasiri,⁴ R. Kumar,³¹ C. C. Kuo,²² Y.-J. Kwon,⁵¹ G. Leder,⁹ J. Lee,³⁷ T. Lesiak,²⁵ J. Li,³⁶
 A. Limosani,⁷ D. Liventsev,¹¹ G. Majumder,⁴¹ F. Mandl,⁹ T. Matsumoto,⁴⁷ W. Mitaroff,⁹ K. Miyabayashi,²¹
 H. Miyake,³⁰ H. Miyata,²⁷ D. Mohapatra,⁵⁰ T. Nagamine,⁴⁴ I. Nakamura,⁷ E. Nakano,²⁹ Z. Natkaniec,²⁵
 S. Nishida,⁷ O. Nitoh,⁴⁸ S. Noguchi,²¹ T. Nozaki,⁷ S. Ogawa,⁴² T. Ohshima,²⁰ S. Okuno,¹³ S. L. Olsen,⁵
 Y. Onuki,²⁷ P. Pakhlov,¹¹ C. W. Park,³⁹ H. Park,¹⁵ L. S. Peak,⁴⁰ R. Pestotnik,¹² L. E. Piilonen,⁵⁰ A. Poluektov,¹
 M. Rozanska,²⁵ Y. Sakai,⁷ N. Sato,²⁰ N. Satoyama,³⁸ K. Sayeed,⁴ T. Schietinger,¹⁶ O. Schneider,¹⁶ A. J. Schwartz,⁴
 R. Seidl,^{6,34} K. Senyo,²⁰ M. E. Sevier,¹⁹ M. Shapkin,¹⁰ H. Shibuya,⁴² B. Shwartz,¹ J. B. Singh,³¹ A. Sokolov,¹⁰
 A. Somov,⁴ N. Soni,³¹ R. Stamen,⁷ S. Stanič,²⁸ M. Starič,¹² H. Stoeck,⁴⁰ K. Sumisawa,³⁰ S. Suzuki,³⁵ S. Y. Suzuki,⁷
 F. Takasaki,⁷ M. Tanaka,⁷ Y. Teramoto,²⁹ X. C. Tian,³² K. Trabelsi,⁵ T. Tsukamoto,⁷ S. Uehara,⁷
 K. Ueno,²⁴ S. Uno,⁷ P. Urquijo,¹⁹ Y. Ushiroda,⁷ Y. Usov,¹ G. Varner,⁵ K. E. Varvell,⁴⁰ S. Villa,¹⁶
 C. H. Wang,²³ Y. Watanabe,⁴⁶ E. Won,¹⁴ Q. L. Xie,⁸ B. D. Yabsley,⁴⁰ A. Yamaguchi,⁴⁴ Y. Yamashita,²⁶
 M. Yamauchi,⁷ J. Ying,³² C. C. Zhang,⁸ L. M. Zhang,³⁶ Z. P. Zhang,³⁶ V. Zhilich,¹ and D. Zürcher¹⁶

(The Belle Collaboration)

¹*Budker Institute of Nuclear Physics, Novosibirsk*

²*Chiba University, Chiba*

³*Chonnam National University, Kwangju*

⁴*University of Cincinnati, Cincinnati, Ohio 45221*

⁵*University of Hawaii, Honolulu, Hawaii 96822*

⁶*University of Illinois at Urbana-Champaign, Urbana, Illinois 61801*

⁷*High Energy Accelerator Research Organization (KEK), Tsukuba*

⁸*Institute of High Energy Physics, Chinese Academy of Sciences, Beijing*

⁹*Institute of High Energy Physics, Vienna*

¹⁰*Institute of High Energy Physics, Protvino*

¹¹*Institute for Theoretical and Experimental Physics, Moscow*

¹²*J. Stefan Institute, Ljubljana*

¹³*Kanagawa University, Yokohama*

¹⁴*Korea University, Seoul*

¹⁵*Kyungpook National University, Taegu*

¹⁶*Swiss Federal Institute of Technology of Lausanne, EPFL, Lausanne*

¹⁷*University of Ljubljana, Ljubljana*

¹⁸*University of Maribor, Maribor*

¹⁹*University of Melbourne, Victoria*

²⁰*Nagoya University, Nagoya*

²¹*Nara Women's University, Nara*

²²*National Central University, Chung-li*

²³*National United University, Miao Li*

²⁴*Department of Physics, National Taiwan University, Taipei*

²⁵*H. Niewodniczanski Institute of Nuclear Physics, Krakow*

²⁶*Nippon Dental University, Niigata*

²⁷*Niigata University, Niigata*

²⁸*Nova Gorica Polytechnic, Nova Gorica*

²⁹*Osaka City University, Osaka*

³⁰*Osaka University, Osaka*

³¹*Panjab University, Chandigarh*

³²*Peking University, Beijing*

³³*Princeton University, Princeton, New Jersey 08544*

³⁴RIKEN BNL Research Center, Upton, New York 11973

³⁵Saga University, Saga

³⁶University of Science and Technology of China, Hefei

³⁷Seoul National University, Seoul

³⁸Shinshu University, Nagano

³⁹Sungkyunkwan University, Suwon

⁴⁰University of Sydney, Sydney NSW

⁴¹Tata Institute of Fundamental Research, Bombay

⁴²Toho University, Funabashi

⁴³Tohoku Gakuin University, Tagajo

⁴⁴Tohoku University, Sendai

⁴⁵Department of Physics, University of Tokyo, Tokyo

⁴⁶Tokyo Institute of Technology, Tokyo

⁴⁷Tokyo Metropolitan University, Tokyo

⁴⁸Tokyo University of Agriculture and Technology, Tokyo

⁴⁹University of Tsukuba, Tsukuba

⁵⁰Virginia Polytechnic Institute and State University, Blacksburg, Virginia 24061

⁵¹Yonsei University, Seoul

We report measurements of time dependent decay rates for $B^0 \rightarrow D^{(*)-}\pi^+$ decays and extraction of CP violation parameters that depend on ϕ_3 . Using fully reconstructed $D^{(*)}\pi$ events and partially reconstructed $D^*\pi$ events from a data sample that contains 386 million $B\bar{B}$ pairs that was collected near the $\Upsilon(4S)$ resonance, with the Belle detector at the KEKB asymmetric energy e^+e^- collider, we obtain the CP violation parameters $S^+(D^{(*)}\pi)$ and $S^-(D^{(*)}\pi)$. We obtain $S^+(D^*\pi) = 0.049 \pm 0.020(\text{stat}) \pm 0.011(\text{sys})$, $S^-(D^*\pi) = 0.031 \pm 0.019(\text{stat}) \pm 0.011(\text{sys})$, and $S^+(D\pi) = 0.031 \pm 0.030(\text{stat}) \pm 0.012(\text{sys})$, $S^-(D\pi) = 0.068 \pm 0.029(\text{stat}) \pm 0.012(\text{sys})$. These results are an indication of CP violation in $B^0 \rightarrow D^{*-}\pi^+$ and $B^0 \rightarrow D^-\pi^+$ decays at the 2.5σ and 2.2σ levels, respectively. If we use the values of $R_{D^{(*)}\pi}$ that are derived using assumptions of factorization and $SU(3)$ symmetry, the branching fraction measurements for the $D_s^{(*)}\pi$ modes, and lattice QCD calculations, we can restrict the allowed region of $|\sin(2\phi_1 + \phi_3)|$ to be above 0.44 and 0.52 at 68% confidence level from the $D^*\pi$ and $D\pi$ modes, respectively.

PACS numbers: 13.65.+i, 13.25.Gv, 14.40.Gx

I. INTRODUCTION

Within the Standard Model (SM), CP violation arises due to a single phase in the Cabibbo-Kobayashi-Maskawa (CKM) quark mixing matrix [1]. Precise measurements of CKM matrix parameters therefore constrain the SM, and may reveal new sources of CP violation. Measurements of the time-dependent decay rates of $B^0(\bar{B}^0) \rightarrow D^{(*)\mp}\pi^\pm$ provide a theoretically clean method for extracting $\sin(2\phi_1 + \phi_3)$ [2]. As shown in Fig. 1, these decays can be mediated by both Cabibbo-favoured decay (CFD) and doubly-Cabibbo-suppressed decay (DCSD) amplitudes, $V_{cb}^*V_{ud}$ and $V_{ub}^*V_{cd}$, which have a relative weak phase ϕ_3 .

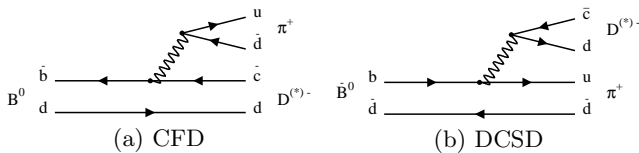


FIG. 1: Diagrams for (a) $B^0 \rightarrow D^{(*)-}\pi^+$ and (b) $\bar{B}^0 \rightarrow D^{(*)-}\pi^+$. Those for $\bar{B}^0 \rightarrow D^{(*)+}\pi^-$ and $B^0 \rightarrow D^{(*)+}\pi^-$ can be obtained by charge conjugation.

The time-dependent decay rates are given by [3]

$$\begin{aligned}
 P(B^0 \rightarrow D^{(*)+}\pi^-) &= \frac{1}{8\tau_{B^0}} e^{-|\Delta t|/\tau_{B^0}} \\
 &\times [1 - C \cos(\Delta m \Delta t) - S^+ \sin(\Delta m \Delta t)], \\
 P(B^0 \rightarrow D^{(*)-}\pi^+) &= \frac{1}{8\tau_{B^0}} e^{-|\Delta t|/\tau_{B^0}} \\
 &\times [1 + C \cos(\Delta m \Delta t) - S^- \sin(\Delta m \Delta t)], \\
 P(\bar{B}^0 \rightarrow D^{(*)+}\pi^-) &= \frac{1}{8\tau_{B^0}} e^{-|\Delta t|/\tau_{B^0}} \\
 &\times [1 + C \cos(\Delta m \Delta t) + S^+ \sin(\Delta m \Delta t)], \\
 P(\bar{B}^0 \rightarrow D^{(*)-}\pi^+) &= \frac{1}{8\tau_{B^0}} e^{-|\Delta t|/\tau_{B^0}} \\
 &\times [1 - C \cos(\Delta m \Delta t) + S^- \sin(\Delta m \Delta t)]. \quad (1)
 \end{aligned}$$

Here Δt is the difference between the time of the decay and the time that the flavour of the B meson is tagged, τ_{B^0} is the average neutral B meson lifetime, Δm is the B^0 - \bar{B}^0 mixing parameter, and $C = (1 - R^2) / (1 + R^2)$, where R is the ratio of the magnitudes of the DCSD and CFD (we assume the magnitudes of both the CFD and DCSD amplitudes are the same for B^0 and \bar{B}^0 decays). The CP violation parameters are given by

$$S^\pm = \frac{2(-1)^L R \sin(2\phi_1 + \phi_3 \pm \delta)}{(1 + R^2)}, \quad (2)$$

where L is the orbital angular momentum of the final state (1 for $D^*\pi$ and 0 for $D\pi$), and δ is the strong phase difference of the CFD and DCSD. The values of R and δ are not necessarily the same for $D^*\pi$ and $D\pi$ final states, and are denoted with subscripts, $D^*\pi$ and $D\pi$, in what follows.

Although not measured yet, the value of R is predicted to be about 0.02 [4]. Therefore, we neglect terms of $\mathcal{O}(R^2)$ (and hence take $C = 1$). There are theoretical arguments that the still unmeasured values of δ for both $D^*\pi$ and $D\pi$ are small [3, 5].

Due to the size of R , CP violation is expected to be a small effect in these decays. Therefore, a large event sample is needed in order to obtain sufficient sensitivity. With this in mind, we employ a partial reconstruction technique [6] for the $D^*\pi$ analysis in addition to the conventional full reconstruction method. In this approach, the signal is distinguished from background on the basis of kinematics of the “fast” pion from the decay $B \rightarrow D^*\pi_f$, and the “slow” pion from the decay $D^* \rightarrow D\pi_s$, alone; no attempt is made to reconstruct the D meson from its decay products. Background from continuum $e^+e^- \rightarrow q\bar{q}$ ($q = u, d, s, c$) events is reduced dramatically by requiring the presence of a high-momentum lepton in the event, which also serves to tag the flavour of the associated B in the event.

Results from our previous analyses using a 140 fb^{-1} data sample containing 152 million $B\bar{B}$ pairs have been published for the full reconstruction method [7] and the partial reconstruction method [8]. Results from similar analyses by BaBar collaboration were also reported [9, 10]. This study is a continuation of similar analyses with a substantially increased data sample containing 386 million $B\bar{B}$ events, and several improvements in the analyses.

II. BELLE DETECTOR

The data was collected with the Belle detector [11] at the KEKB asymmetric energy electron-positron collider [12] operating at the $\Upsilon(4S)$ resonance. The Belle detector is a large-solid-angle magnetic spectrometer that consists of a silicon vertex detector (SVD), a 50-layer central drift chamber (CDC), an array of aerogel threshold Cherenkov counters (ACC), a barrel-like arrangement of time-of-flight scintillation counters (TOF), and an electromagnetic calorimeter (ECL) comprised of CsI(Tl) crystals located inside a superconducting solenoidal coil that provides a 1.5 T magnetic field. An iron flux-return located outside of the coil is instrumented to detect K_L^0 mesons and to identify muons (KLM). A sample containing 152 million $B\bar{B}$ pairs was collected with a 2.0 cm radius beampipe and a 3-layer silicon vertex detector (SVD1), while a sample of 234 million $B\bar{B}$ pairs was collected with a 1.5 cm radius beampipe, a 4-layer silicon detector, and a small-cell inner drift chamber (SVD2) [13].

III. FULL RECONSTRUCTION ANALYSIS

A. Signal Event Selection

The selection of hadronic events is described elsewhere [14]. For the $\bar{B}^0 \rightarrow D^{*+}\pi^-$ event selection, we use the decay chain $D^{*+} \rightarrow D^+\pi^0$ or $D^0\pi^+$ with subsequent decays of $D^+ \rightarrow K^-\pi^+\pi^+$ and $D^0 \rightarrow K^-\pi^+$, $K^-\pi^+\pi^0$, $K^-\pi^+\pi^+\pi^-$, $K_S^0\pi^+\pi^-$ ($K_S^0 \rightarrow \pi^+\pi^-$). (Charge conjugate modes are implied throughout this Paper.) All charged tracks except for the slow pions from $D^* \rightarrow D\pi$ decays are required to have a minimum of one hit (two hits) in the r - ϕ (z) coordinate of the vertex detector, where the r - ϕ plane is transverse to the positron beam line that defines the z axis. These requirements allow a precise determination of the production point. To separate kaons from pions, we form a likelihood for each track, $\mathcal{L}_{K(\pi)}$. The kaon likelihood ratio, $P(K/\pi) = \mathcal{L}_K/(\mathcal{L}_K + \mathcal{L}_\pi)$, has values between 0 (likely to be a pion) and 1 (likely to be a kaon). We require charged kaons to satisfy $P(K/\pi) > 0.3$, corresponding to about 95% efficiency for detecting kaons and about 2% probability for misidentifying pions as kaons. There is no such requirement for charged pions coming from D decays.

Neutral pions are formed from photon pairs with invariant masses between $0.118\text{ GeV}/c^2$ and $0.150\text{ GeV}/c^2$. The photon momenta are then recalculated with a π^0 mass constraint.

We require the invariant mass of $K_S^0 \rightarrow \pi^+\pi^-$ candidates to be between $0.485\text{ GeV}/c^2$ and $0.510\text{ GeV}/c^2$ corresponding to $\pm 5\sigma$, where σ is the Monte Carlo (MC) determined invariant mass resolution. The radial impact parameter, which is the distance of closest approach of the candidate charged tracks to the event-dependent interaction point (IP) in the r - ϕ plane, is required to be larger than 0.02 cm for high momentum ($> 1.5\text{ GeV}/c$) K_S^0 candidates and 0.03 cm for those with momentum less than $1.5\text{ GeV}/c$. Here the IP is determined for each set of 10,000 neighboring hadronic events, and the K_S^0 momentum is given in the $\Upsilon(4S)$ rest frame (cms). The $\pi^+\pi^-$ vertex is required to be displaced from the IP by a minimum transverse distance of 0.22 cm for high momentum candidates and 0.08 cm for the remaining candidates. The mismatch in the z direction at the K_S^0 vertex point for the $\pi^+\pi^-$ tracks must be less than 2.4 cm for high momentum candidates and 1.8 cm for the remaining candidates. The direction of the pion pair momentum must also agree with the direction of the vertex point from the IP to within 0.03 rad for high momentum candidates and to within 0.1 rad for the remaining candidates. A mass and vertex constraint is imposed when fitting the K_S^0 candidates.

For D^0 meson candidates, the invariant mass of the D^0 candidate is required to be within ± 20 , ± 30 , ± 20 , and $\pm 20\text{ MeV}/c^2$ for $K^-\pi^+$, $K^-\pi^+\pi^0$, $K^-\pi^+\pi^+\pi^-$, $K_S^0\pi^+\pi^-$ modes respectively, while the invariant mass of the D^+ candi-

dates should be within $\pm 18 \text{ MeV}/c^2$ of the nominal D^+ mass corresponding to $\pm 4\sigma$. For the $D^0 \rightarrow K^-\pi^+\pi^0$ mode, we further require the π^0 cms momentum to be greater than $200 \text{ MeV}/c$. We use a mass- and vertex-constrained fit for D candidates.

The D^{*+} is reconstructed by combining either D^0 candidates with a slow π^+ meson, or D^+ candidates with a slow π^0 meson. The D^* candidates are required to have a mass difference $\Delta M = M_{D\pi} - M_D$ within $\pm 3 \text{ MeV}/c^2$ to $\pm 5 \text{ MeV}/c^2$ of the nominal value depending on the decay mode.

We reconstruct a B candidate by combining the $D^{(*)+}$ candidate with a π^- candidate satisfying $P(K/\pi) < 0.8$, corresponding to more than 90% efficiency for detecting pions and less than 10% probability for misidentifying kaons as pions. We identify B decays based on requirements on the energy difference $\Delta E \equiv \sum_i E_i - E_{\text{beam}}$ and the beam-energy constrained mass $M_{\text{bc}} \equiv \sqrt{E_{\text{beam}}^2 - (\sum_i \vec{p}_i)^2}$, where E_{beam} is the beam energy, and \vec{p}_i and E_i are the momenta and energies of the daughters of the reconstructed B meson candidate, all in the cms. We define a signal region in the ΔE - M_{bc} plane of $5.27 \text{ GeV}/c^2 < M_{\text{bc}} < 5.29 \text{ GeV}/c^2$ and $|\Delta E| < 0.045 \text{ GeV}$, corresponding to about $\pm 3\sigma$ on each quantity. If more than one B candidate is found in the same event, we select the one with best D vertex quality. For the determination of background parameters, we use events in a sideband region defined by $M_{\text{bc}} > 5.2 \text{ GeV}/c^2$ and $-0.14 \text{ GeV} < \Delta E < 0.20 \text{ GeV}$, excluding the signal region.

The ΔE and M_{bc} distributions for $D^*\pi$ and $D\pi$ candidates are shown in Fig. 2. A study using MC events indicates the presence of “peaking background” that peaks in the signal ΔE - M_{bc} region and amounts to 1.7% (0.7%) of the $D^*\pi$ ($D\pi$) candidates, respectively. We treat this contribution as a part of the signal, and assign a systematic error to account for this.

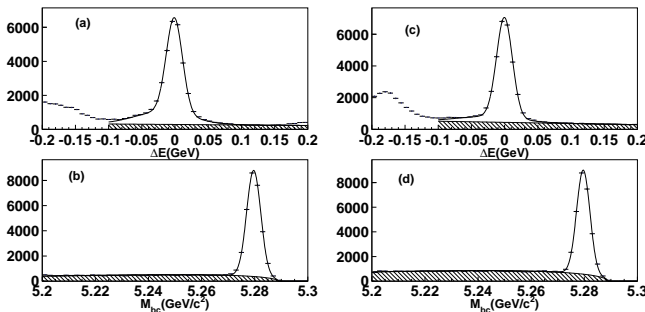


FIG. 2: ΔE and M_{bc} distributions for $B^0 \rightarrow D^{*+}\pi^-$ candidates (a and b), and $B^0 \rightarrow D^+\pi^-$ candidates (c and d). Curves are the fit results. Hatched regions indicate the background components of the fits.

B. Flavour Tagging

Charged leptons, pions, and kaons that are not associated with the reconstructed $D^{(*)}\pi$ decays are used to identify the flavour of the accompanying B meson. The algorithm [15] produces two parameters for each event, q and r , where $q = +1$ ($q = -1$) for a B^0 (\bar{B}^0) meson and r is a quality factor ranging from 0 for no flavour discrimination to 1 for unambiguous flavour assignment. The algorithm uses the kinematical variables of the event and compares to those from a large number of MC events, and is used only to sort the data into six intervals of r according to estimated flavour purity. More than 99.5% of the events are assigned non-zero values of r .

C. Vertex Measurement

The decay vertex of the $B \rightarrow D^{(*)}\pi$ candidate is fitted using the track information of the D and π (except the slow π from D^* decay). For the decay vertex of the tagging B meson, the remaining well-reconstructed tracks in the event are used. Tracks that are consistent with K_S^0 decay are rejected. We impose the additional requirement that both signal-side and tagging-side vertices be consistent with the run-dependent IP profile. A study using a MC event sample shows that the nominal χ^2 of the vertex reconstruction is strongly correlated with the distance from the IP to the reconstructed vertex. To avoid possible bias in the event selection due to this correlation, we introduce a quantity that only depends on the z coordinate quantities;

$$\xi \equiv \frac{1}{2n} \sum_i^n \left| \frac{z_i^{\text{after}} - z_i^{\text{before}}}{\epsilon_i^{\text{before}}} \right|^2, \quad (3)$$

where n is the number of tracks, z_i are the z vertices of the i -th track before and after the vertex fit, and $\epsilon_i^{\text{before}}$ is the measurement error of the z before the vertex fit. This quantity is calculated for the signal- and tagging-side separately, only for cases with multiple tracks. We require $\xi < 100$ to eliminate badly reconstructed vertices, which amount to 4% (2%) of the signal-side and 1% (1%) of the tagging-side in the $D^*\pi$ and $D\pi$ modes, respectively.

The proper-time difference between the vertices z_{rec} and z_{tag} (measured along the beam line) of the fully reconstructed B candidate and the tagging B meson, respectively, is calculated as

$$\Delta t = (z_{\text{rec}} - z_{\text{tag}})/\beta\gamma c, \quad (4)$$

where $\beta\gamma = 0.425$ is the Lorentz boost factor of the centre of mass frame at KEKB. After application of the event selection criteria and the requirement that both B mesons have well defined vertices and $|\Delta t| < 70 \text{ ps}$ ($\sim 45 \tau_{B^0}$), 31491 and 31725 candidates remain in the $D^*\pi$ and $D\pi$

modes, respectively. The signal fractions of the candidates, which vary for different r bins, are 89% for $D^*\pi$ and 83% for $D\pi$.

D. Δt Fit

Unbinned maximum likelihood fits to the four time dependent decay rates are performed to extract S^+ and S^- . We minimize $-2 \sum_i \ln \mathcal{L}_i$ where the likelihood for the i -th event is given by

$$\mathcal{L}_i = (1 - f_{\text{ol}}) [f_{\text{sig}} P_{\text{sig}} + (1 - f_{\text{sig}}) P_{\text{bkg}}] + f_{\text{ol}} P_{\text{ol}}. \quad (5)$$

The signal fraction f_{sig} is determined from the $(\Delta E - M_{\text{bc}})$ value of each event. The signal distribution is the product of the sum of two Gaussians in ΔE and a Gaussian in M_{bc} ; that for the background is the product of a first order polynomial in ΔE and an ARGUS function [16] in M_{bc} .

The signal Δt distribution is given by

$$P(q = -1, D^{(*)\pm} \pi^\mp) = (1 - w_-) P(B^0 \rightarrow D^{(*)\pm} \pi^\mp) + w_+ P(\bar{B}^0 \rightarrow D^{(*)\pm} \pi^\mp) \quad (6)$$

for the $q = -1$ sample, and

$$P(q = +1, D^{(*)\pm} \pi^\mp) = (1 - w_+) P(\bar{B}^0 \rightarrow D^{(*)\pm} \pi^\mp) + w_- P(B^0 \rightarrow D^{(*)\pm} \pi^\mp) \quad (7)$$

for the $q = +1$ sample. Here w_+ and w_- are respectively the probabilities to incorrectly assign the flavour of tagging B^0 and \bar{B}^0 mesons (wrong tag fractions), and the decay rates are given by Eq. 1.

The corresponding background distribution is parameterized as a sum of a δ -function component and an exponential component with lifetime τ_{bkg} :

$$\delta(\Delta t - \mu_{\text{bkg}}^\delta) + \frac{(1 - f_{\text{bkg}}^\delta)}{2\tau_{\text{bkg}}} e^{-|\Delta t - \mu_{\text{bkg}}^\tau|/\tau_{\text{bkg}}}, \quad (8)$$

where f_{bkg}^δ is the fraction of events contained in the δ -function, μ_{bkg}^δ and μ_{bkg}^τ are the mean values of Δt in the δ -function and exponential components, respectively. These parameters are determined separately from a fit to the Δt distribution in the $\Delta E - M_{\text{bc}}$ sideband data for the $D^*\pi$ and $D\pi$ data samples, SVD1 and SVD2 data, and cases where the vertices are reconstructed using single track and multiple tracks. Typically, values of the background Δt parameters are: $f_{\text{bkg}}^\delta \approx 0.4$, $\tau_{\text{bkg}} \approx 1.1$ ps, $\mu_{\text{bkg}}^\tau \approx -0.1$ ps, and $\mu_{\text{bkg}}^\delta \approx 0$.

A small number of events have poorly reconstructed vertices resulting in very broad Δt distributions. We account for this outlier contribution by adding a Gaussian component P_{ol} with a width and fraction determined from the B lifetime analysis [23].

E. Δt Resolution

The probability density functions (PDF) for the signal and background must be convolved with corresponding Δt resolution functions, that are determined on an event-by-event basis using the estimated uncertainties on the z vertex positions [17, 23], in order to be compared with the data. The signal resolution function is a convolution of three contributions: resolution functions for vertex reconstruction, smearing due to non-primary tracks (K_S^0 and charm daughters), and the kinematic approximation that the B mesons are at rest in the cms. The resolution function is described in detail elsewhere [23].

The background resolution function is parametrized as a sum of two Gaussians where different values are used for the parameters depending on whether or not both vertices are reconstructed with multiple tracks. These parameters are determined from the $\Delta E - M_{\text{bc}}$ sideband data.

F. Tagging Side CP Violation Effect

While the tagging side should have no asymmetry if the flavour is tagged by primary leptons since semileptonic decays are flavour-specific processes, it is possible to introduce a small asymmetry when daughter particles of hadronic decays such as $D^{(*)}\pi$ are used for the flavour tagging, due to the same CP violating effect that is the subject of this paper [18]. This effect is taken into account by replacing the S^\pm parameters in Eq. 1 by

$$\begin{aligned} B^0 \rightarrow D^{(*)+} \pi^- &: S^+ \rightarrow (S^+ - S_{\text{tag}}^+), \\ B^0 \rightarrow D^{(*)-} \pi^+ &: S^- \rightarrow (S^- + S_{\text{tag}}^+), \\ \bar{B}^0 \rightarrow D^{(*)+} \pi^- &: S^+ \rightarrow (S^+ + S_{\text{tag}}^-), \\ \bar{B}^0 \rightarrow D^{(*)-} \pi^+ &: S^- \rightarrow (S^- - S_{\text{tag}}^-), \end{aligned} \quad (9)$$

respectively. Here S_{tag}^+ and S_{tag}^- represent the CP violation effect on the flavour tagging side due to the presence of $B^0 \rightarrow \bar{D} \bar{X}$ and $\bar{B}^0 \rightarrow DX$ amplitudes, respectively. Note that unlike the S^\pm parameters, which are defined rigorously in terms of $B^0 \rightarrow D^{(*)\mp} \pi^\pm$ and $\bar{B}^0 \rightarrow D^{(*)\pm} \pi^\mp$ amplitudes, S_{tag}^\pm are effective quantities that include effects of the fraction of $B \rightarrow DX(\bar{D} \bar{X})$ components in the tagging B decays and the subsequent behaviour of $D(\bar{D})$ mesons. Therefore, these quantities must be determined experimentally.

The values of S_{tag}^\pm are determined in each r bin by fitting the Δt distributions of a $B \rightarrow D^* l \nu$ control sample [15] using the signal PDFs of Eqs. 6 and 7 and setting S^\pm to zero. Since the $D^* l \nu$ final states have specific flavour, any observable asymmetry must originate from the tagging side. The results for each r bin are listed in Table I. The errors listed here are statistical only. The result for the combined r bins are $S_{\text{tag}}^+ = -0.002 \pm 0.009 \pm 0.006$ and $S_{\text{tag}}^- = 0.017 \pm 0.009 \pm 0.006$, where the second errors are systematic.

TABLE I: Parameters describing tagging side CP violation effect that are determined from the $D^*\nu$ data sample.

r	S_{tag}^+	S_{tag}^-
0.000 – 0.250	-0.058 ± 0.130	$+0.060 \pm 0.130$
0.250 – 0.500	$+0.001 \pm 0.040$	$+0.018 \pm 0.040$
0.500 – 0.625	$+0.027 \pm 0.032$	-0.030 ± 0.032
0.625 – 0.750	$+0.026 \pm 0.025$	$+0.022 \pm 0.025$
0.750 – 0.875	-0.011 ± 0.025	$+0.027 \pm 0.025$
0.875 – 1.000	-0.005 ± 0.014	$+0.024 \pm 0.014$

G. Fit Result

The procedures for Δt determination and flavour tagging are tested by extracting τ_{B^0} and Δm . When all four signal categories in Eq. 1 are combined, the signal Δt distribution reduces to an exponential lifetime distribution as shown in Fig. 3(a). We do a simultaneous fit to the SVD1 and SVD2 samples by combining the $D^*\pi$ and $D\pi$ candidate events and obtain $\tau_{B^0} = 1.532 \pm 0.013$ ps, where the error is statistical only, in good agreement with the world average of 1.536 ± 0.014 ps [19]. Combining the two CFD-dominant modes (denoted as OF because the signal-side and tagging-side have opposite B flavour) and the two mixing-dominant modes (denoted as SF because the signal-side and tagging-side have same B flavour) and ignoring the CP violating terms, an asymmetry $(\text{OF} - \text{SF})/(\text{OF} + \text{SF})$ behaves as $\cos(\Delta m \Delta t)$ as shown in Fig. 3(b). A similar fit to the one used for the lifetime determination gives $\Delta m = 0.494 \pm 0.007$ ps $^{-1}$, where the error is statistical only, also in good agreement with the world average 0.502 ± 0.007 ps $^{-1}$ [19]. This fit is also used to determine the signal Δt resolution parameters and wrong tag fractions w_+ and w_- in each r bin for both SVD1 and SVD2 samples. Table II lists the fit result for the wrong tag fractions in the SVD2 sample. Those from the SVD1 sample have very similar values.

TABLE II: Fit results for the wrong tag fractions of the SVD2 sample. They are determined in each r bin as the averages and differences of the two flavours.

r	$(w_+ + w_-)/2$	$(w_+ - w_-)$
0.000 – 0.250	0.461 ± 0.006	$+0.001 \pm 0.009$
0.250 – 0.500	0.327 ± 0.009	-0.026 ± 0.013
0.500 – 0.625	0.216 ± 0.010	$+0.032 \pm 0.015$
0.625 – 0.750	0.163 ± 0.009	-0.001 ± 0.014
0.750 – 0.875	0.124 ± 0.009	-0.020 ± 0.014
0.875 – 1.000	0.032 ± 0.005	$+0.012 \pm 0.009$

We then perform fits to determine the values of S^\pm by fixing τ_{B^0} and Δm_d to the world average values and using previously determined w_\pm and S_{tag}^\pm in each r bin. The results are $S^+(D^*\pi) = 0.050 \pm 0.029$, $S^-(D^*\pi) = 0.028 \pm 0.028$, $S^+(D\pi) = 0.031 \pm 0.030$, and $S^-(D\pi) = 0.068 \pm 0.029$. The errors are statistical only.

The Δt distributions for the subsamples having the

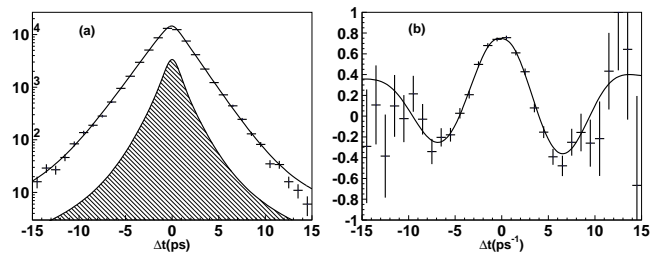


FIG. 3: (a) Δt distribution for the signal candidates when all four signal categories are combined. (b) $(\text{OF} - \text{SF})/(\text{OF} + \text{SF})$ asymmetries. Curves are the fit results. The hatched region in (a) indicates the background.

best quality flavour tagging ($0.875 < r \leq 1.0$) are shown in Fig. 4 for the $D^*\pi$ mode and in Fig. 5 for the $D\pi$ mode. For both modes, this region constitutes roughly 14% of the total, but has significant statistical power for the S^\pm determination.

H. Systematic Error

The systematic errors come from the uncertainties of parameters that are constrained in the fit (Δt resolution, background Δt shape, background fractions, wrong tag fractions, vertexing, physics parameters), uncertainties due to the tag side asymmetry and biases induced by the fitting method. To estimate contributions from the fit parameter uncertainties, we repeat the fit by varying each parameter by a given amount, and assign the shift in the S^\pm parameters from the nominal fit as a systematic error. The signal Δt resolution parameters are varied by $\pm 1\sigma$ of their errors. The background Δt shape parameters are varied by $\pm 1\sigma$ of their errors. For the background fraction, in addition to varying the parameters of the ΔE - M_{bc} signal region fit by $\pm 1\sigma$, we vary the ΔE signal region cut by ± 5 MeV and M_{bc} signal region cut by ± 3 MeV/ c^2 and the quadratic sum of these is assigned as an error. Contributions from the peaking background are found to be negligible based on a MC study. We vary the wrong tag fraction parameters by $\pm 1\sigma$ in each r bin and add in quadrature. We vary the cut of ξ by +100 and -50, which gives 0.004 for $D^*\pi$ and 0.002 for $D\pi$ as errors due to the vertexing. We repeat the fit after removing the $|\Delta t| < 70$ ps cut and find a negligible shift. We vary the errors for τ_{B^0} and Δm by $\pm 1\sigma$.

For the tag side asymmetry, the quadratic sum of statistical and systematic errors of S_{tag}^\pm parameters are varied by $\pm 1\sigma$ in each r bin and the deviations are added in quadrature, giving 0.005 as an error. Since this error includes contributions from unknown effects in the vertex measurement such as the misalignment of the SVD and drift of the IP profile, we do not explicitly assign additional error to the vertexing other than that from the ξ cut.

Fit bias is tested using a $D^*\pi$ signal MC sample where

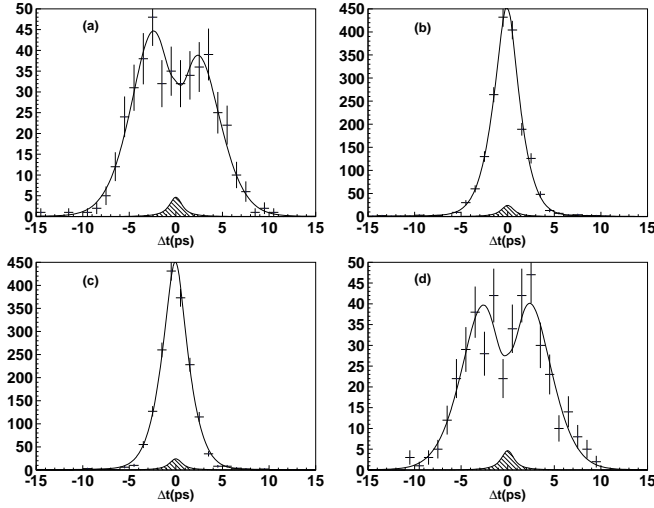


FIG. 4: Δt distributions for the $D^*\pi$ events in the $0.875 < r \leq 1.0$ flavour tagging quality bin. (a) $B^0 \rightarrow D^{*+}\pi^-$, (b) $B^0 \rightarrow D^{*-}\pi^+$, (c) $\bar{B}^0 \rightarrow D^{*+}\pi^-$, (d) $\bar{B}^0 \rightarrow D^{*-}\pi^+$. Curves show the results of fits to the entire event sample, and hatched regions indicate the backgrounds.

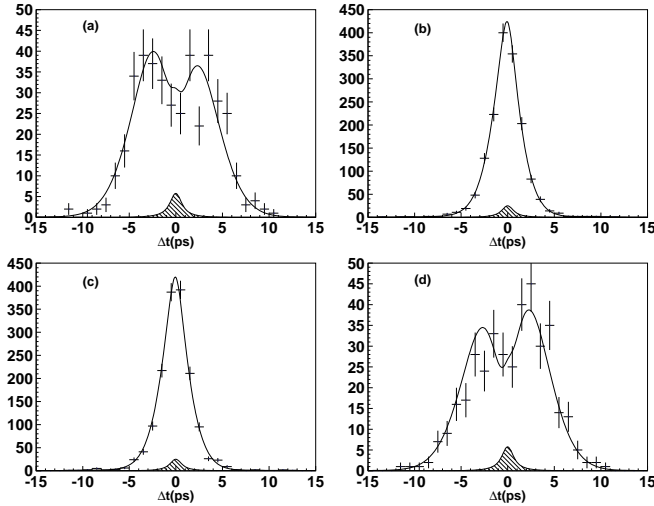


FIG. 5: Δt distributions for the $D\pi$ events in the $0.875 < r \leq 1.0$ flavour tagging quality bin. (a) $B^0 \rightarrow D^+\pi^-$, (b) $B^0 \rightarrow D^-\pi^+$, (c) $\bar{B}^0 \rightarrow D^+\pi^-$, (d) $\bar{B}^0 \rightarrow D^-\pi^+$. Curves show the results of fits to the entire event sample, and hatched regions indicate the backgrounds.

one B meson decays to $D^*\pi$, and the other B decays generically. We fit the S^\pm parameter to this sample, with and without the S_{tag}^\pm correction given in Eq. 9, taking S_{tag}^\pm values from a $B \rightarrow D^*\nu$ signal MC sample. Neither MC sample includes the tag side CP violation effects, so the two fits should return the same S^\pm values in principle. We take the difference between the fits, 0.010, as a measure of biases in the fitting procedure.

We obtain a total systematic error of 0.013 for $D^*\pi$ and 0.012 for $D\pi$. Table III summarizes the contributions to the systematic errors.

TABLE III: Summary of the systematic errors in the S^\pm measurements using the full reconstruction method.

Sources	$D^*\pi$	$D\pi$
Signal Δt resolution	0.005	0.004
Background Δt shape	negligible	negligible
Background fraction	0.002	0.001
Wrong tag fraction	0.002	0.002
Vertexing	0.004	0.002
Physics parameters ($\Delta m, \tau_{B^0}$)	0.001	0.001
Tag side asymmetry	0.005	0.005
Fit bias	0.010	0.010
Total	0.013	0.012

I. Result

We obtain

$$\begin{aligned}
 S^+(D^*\pi) &= 0.050 \pm 0.029 \pm 0.013, \\
 S^-(D^*\pi) &= 0.028 \pm 0.028 \pm 0.013, \\
 S^+(D\pi) &= 0.031 \pm 0.030 \pm 0.012, \\
 S^-(D\pi) &= 0.068 \pm 0.029 \pm 0.012
 \end{aligned} \tag{10}$$

from the full reconstruction method, where the first error is statistical and the second error is systematic.

IV. PARTIAL RECONSTRUCTION ANALYSIS

A. Signal Event Selection

Candidate events are selected by requiring the presence of fast pion and slow pion candidates. In order to obtain accurate vertex position determinations, fast pion candidates are required to have a radial (longitudinal) impact parameter $dr < 0.1$ cm ($|dz| < 2.0$ cm), to have associated hits in the SVD, and to have a polar angle in the laboratory frame in the range $30^\circ < \theta_{\text{lab}} < 135^\circ$. The vertex positions are obtained by fits of the candidate tracks with the IP. Fast pion candidates are required to be inconsistent with the lepton hypothesis (see below), and the kaon hypothesis, based on information from the CDC, TOF and ACC. A requirement on the fast pion cms momentum of $1.83 \text{ GeV}/c < p_{\pi_f} < 2.43 \text{ GeV}/c$ is made; this range includes both signal and sideband regions (defined below). Slow pion candidates are required to have cms momentum in the range $0.05 \text{ GeV}/c < p_{\pi_s} < 0.30 \text{ GeV}/c$. No requirement is made on particle identification for slow pions; since they are not used for vertexing, only a loose requirement that they originate from the IP is made. The fast and slow pion candidates must have opposite charges.

B. Flavour Tagging

In order to tag the flavour of the associated B meson and to reduce background from continuum $e^+e^- \rightarrow$

$q\bar{q}$ ($q = u, d, s, c$) processes, we require the presence of a high-momentum lepton in the event. Tagging lepton candidates are required to be positively identified either as electrons, on the basis of information from the CDC, ECL and ACC, or as muons, on the basis of information from the CDC and the KLM. They are required to have momentum in the range $1.2 \text{ GeV}/c < p_{l_{\text{tag}}} < 2.3 \text{ GeV}/c$, and to have an angle with the fast pion candidate that satisfies $-0.75 < \cos \delta_{\pi_f l}$ in the cms. The lower bound on the momentum and the requirement on the angle also reduce, to a negligible level, the contribution of leptons produced from semi-leptonic decays of the unreconstructed D mesons in the $B^0 \rightarrow D^{*\mp} \pi^\pm$ decay chain. No other tagging lepton candidate with momentum greater than $1.0 \text{ GeV}/c$ is allowed in the event to reduce the mistagging probability, and also to reduce the contribution from leptonic charmonium decays. Identical vertexing requirements to those for fast pion candidates are made in order to obtain an accurate z_{tag} position. To further suppress the small remaining continuum background, we impose a loose requirement on the ratio of the second to zeroth Fox-Wolfram [20] moments, $R_2 < 0.6$.

C. Kinematic Fit

Signal events are distinguished from background using three kinematic variables, which are approximately independent for signal. These are denoted by p_{π_f} , $\cos \delta_{\pi_f \pi_s}$ and $\cos \theta_{\text{hel}}$. For signal, the fast pion cms momentum, p_{π_f} , has a uniform distribution, smeared by the experimental resolution, as the fast pion is monoenergetic in the B rest frame. The cosine of the angle between the fast pion direction and the opposite of the slow pion direction in the cms, $\cos \delta_{\pi_f \pi_s}$, peaks sharply at +1 for signal, as the slow pion follows the D^* direction due to the small energy released in the D^* decay. The cosine of the angle between the slow pion direction and the opposite of the B direction in the D^* rest frame, $\cos \theta_{\text{hel}}$, has a distribution proportional to $\cos^2 \theta_{\text{hel}}$ for signal events, as the B decay is a pseudoscalar to pseudoscalar vector transition. Since the D^* is not fully reconstructed, $\cos \theta_{\text{hel}}$ is calculated using kinematic constraints, and the background can populate the unphysical region $|\cos \theta_{\text{hel}}| > 1$.

We select candidates that satisfy $1.93 \text{ GeV}/c < p_{\pi_f} < 2.43 \text{ GeV}/c$, $0.850 < \cos \delta_{\pi_f \pi_s} < 1.000$ and $-1.70 < \cos \theta_{\text{hel}} < 1.80$. In the cases where more than one candidate satisfies these criteria, we select the one with the largest value of $\cos \delta_{\pi_f \pi_s}$. We further define signal regions in p_{π_f} and $\cos \delta_{\pi_f \pi_s}$ as $2.13 \text{ GeV}/c < p_{\pi_f} < 2.43 \text{ GeV}/c$, $0.925 < \cos \delta_{\pi_f \pi_s} < 1.000$, and two regions in $\cos \theta_{\text{hel}}$: $-1.00 < \cos \theta_{\text{hel}} < -0.30$ and $+0.40 < \cos \theta_{\text{hel}} < +1.10$.

Background events are separated into three categories: $D^{*\mp} \rho^\pm$, which is kinematically similar to the signal; correlated background, in which the slow pion originates from the decay of a D^* that in turn originates from the decay of the same B candidate as the fast pion candidate (*e.g.*, $D^{**} \pi$); and uncorrelated background, which

includes everything else (*e.g.*, continuum processes, $D\pi$). The kinematic distributions of the background categories and the signal are determined from a large MC sample, corresponding to two times the integrated luminosity of our data sample, in which the branching fractions of the signal and major background sources are weighted according to the most recent knowledge [19, 21]. We also use this MC sample for various tests of the analysis algorithms.

Event-by-event signal fractions are determined from binned maximum likelihood fits to the three-dimensional kinematic distributions (6 bins of $p_{\pi_f} \times 5$ bins of $\cos \delta_{\pi_f \pi_s} \times 10$ bins of $\cos \theta_{\text{hel}}$). The results of these fits, projected onto each of the three variables, are shown in Fig. 6, and summarized in Table IV.

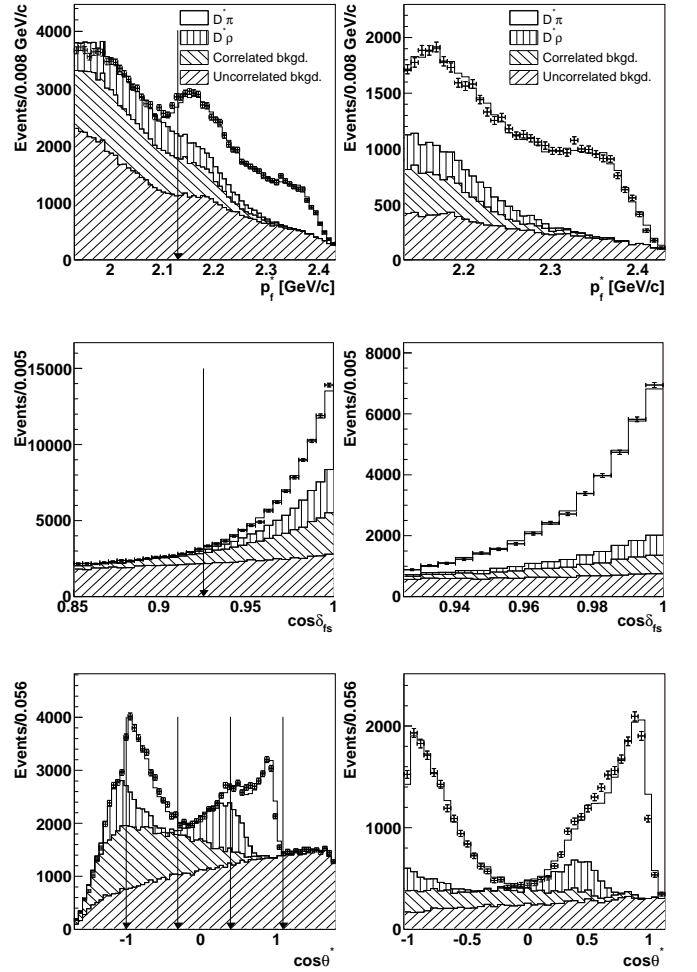


FIG. 6: Results of the kinematic fits to $D^* \pi$ candidates, projected onto (top) the p_{π_f} axis, (middle) the $\cos \delta_{\pi_f \pi_s}$ axis and the (bottom) $\cos \theta_{\text{hel}}$ axis, in both (left) selection region and (right) signal region. The arrows show the edges of the signal regions.

TABLE IV: Summary of the results of the three-dimensional fits to kinematic variables. The numbers of events and fractions given for each category are those extrapolated to inside the signal regions in all three variables. The errors on the fractions are returned by the fit and propagated to the corresponding numbers of events.

	Candidates	Fraction
Data	32844 ± 181	—
$D^*\pi$	21741 ± 217	0.662 ± 0.007
$D^*\rho$	2091 ± 45	0.064 ± 0.001
Correlated background	2703 ± 42	0.082 ± 0.001
Uncorrelated background	6287 ± 40	0.191 ± 0.001

D. Δt Fit Procedure

In order to measure the CP violation parameters in the $D^*\pi$ sample, we perform a simultaneous unbinned fit to the same-flavor (SF) events, in which the fast pion and the tagging lepton have the same charge, and opposite-flavor (OF) events, in which the fast pion and the tagging lepton have the opposite charge. We minimize the quantity $-2 \ln \mathcal{L} = -2 \sum_i \ln \mathcal{L}_i$, where

$$\mathcal{L}_i = f_{D^*\pi} P_{D^*\pi} + f_{D^*\rho} P_{D^*\rho} + f_{\text{unco}} P_{\text{unco}} + f_{\text{corr}} P_{\text{corr}}. \quad (11)$$

The event-by-event signal and background fractions (the f terms) are taken from the results of the kinematic fits. Each P term contains an underlying physics PDF, with experimental effects taken into account. For $D^*\pi$ and $D^*\rho$, the PDF is given by Eq. 1, where for $D^*\rho$ the terms S^\pm are effective parameters averaged over the helicity states [22] that are constrained to be zero. The PDF for correlated background contains a term for neutral B decays (given by Eq. 1 with $S^\pm = 0$), and, in the case of OF events, a term for charged B decays (for which the PDF is $\frac{1}{2\tau_{B^+}} e^{-|\Delta t|/\tau_{B^+}}$, where τ_{B^+} is the lifetime of the charged B meson).

The PDF for uncorrelated background also contains neutral and charged B components, with the remainder from continuum $e^+e^- \rightarrow q\bar{q}$ ($q = u, d, s, c$) processes. The continuum PDF is modelled with two components: one with negligible lifetime, and the other with a finite lifetime. The sideband parameters are determined from data sidebands, as described later.

As mentioned above, experimental effects need to be taken into account to obtain the P terms of Eq. 11. Mistagging is taken into account using

$$\begin{aligned} P(l_{\text{tag}}^-, \pi_f^\pm) &= \\ & (1 - w_-) P(B^0 \rightarrow D^{*\mp} \pi^\pm) + w_+ P(\bar{B}^0 \rightarrow D^{*\mp} \pi^\pm) \\ P(l_{\text{tag}}^+, \pi_f^\pm) &= \\ & (1 - w_+) P(\bar{B}^0 \rightarrow D^{*\mp} \pi^\pm) + w_- P(B^0 \rightarrow D^{*\mp} \pi^\pm), \end{aligned} \quad (12)$$

where w_+ and w_- are the wrong tag fractions, and are determined from the data as free parameters in the fit for S^\pm . It should be noted that the w_+ and w_- values used here are different from those used in the full reconstruction methods because the flavour-tagging methods differ in two cases.

The time difference Δt is related to the measured quantity Δz as described in Eq. 4, with an additional term due to possible offsets in the mean value of Δz ,

$$\Delta t \rightarrow \Delta t + \epsilon_{\Delta t} \simeq (\Delta z + \epsilon_{\Delta z}) / \beta \gamma c. \quad (13)$$

It is essential to allow non-zero values of ϵ since a small bias can mimic the effect of CP violation:

$$\cos(\Delta m \Delta t) \rightarrow \cos(\Delta m \Delta t) - \Delta m \epsilon_{\Delta t} \sin(\Delta m \Delta t). \quad (14)$$

A bias as small as $\epsilon_{\Delta z} \sim 1 \mu\text{m}$ can lead to sine-like terms as large as 0.01, comparable to the expected size of the CP violation effect. We allow separate offsets for each combination of fast pion and tagging lepton charges. We also apply a small correction to each measured vertex position to correct for a known bias due to the relative misalignment of the SVD and CDC in SVD1 data. This correction is dependent on the track charge, momentum and polar angle, measured in the laboratory frame. It is obtained by comparing the vertex positions calculated with the alignment constants used in the data, to those obtained with an improved set of alignment constants [24]. The alignment in SVD2 data was found to be comparable to that of the corrected SVD1 data. No additional correction was thus applied to SVD2 data.

E. Δt Resolution

Resolution effects are taken into account in a way similar to our full reconstruction analysis. The algorithm includes components related to detector resolution, kinematic smearing and non-primary tracks.

For correctly tagged signal events, both the fast pion and the tagging lepton originate directly from B meson decays. Therefore we do not include any additional smearing due to non-primary tracks in these events. Incorrectly tagged events, however, almost exclusively originate from secondary leptons. Furthermore, due to the kinematic constraints on the momentum of the fast pion, secondary tracks consist almost exclusively of wrong-tag leptons. Only uncorrelated background events contain a small amount of secondary pions, which also give the wrong flavour information. In order to take this effect into account, the PDFs of incorrectly tagged events are convolved with an additional resolution component whose parameters are determined from MC simulations. Three different sets of parameters are used: one set for uncorrelated background in the uncorrelated background sideband, where the fast pion momentum cut is loosened; one set for uncorrelated background in the two other regions (signal region and correlated background

side-band); one set for all other categories of events (signal, $D^*\rho$ and correlated background), which contain similar amounts of secondary leptons, and no secondary pions. Because of the aforementioned correlation between mistagging and non-primary tracks, each of these sets are linked to different wrong-tag fractions w_{\pm} .

The effect of the approximation that the B mesons are at rest in the cms in Eq. 4 is taken into account [23]. We use a slightly modified algorithm to describe the detector resolution, in order to precisely describe the observed behaviour for single track vertices. The resolution for each track is described by the sum of three Gaussian components, with a common mean of zero, and widths that are given by the measured vertex error for each track multiplied by different scale factors.

We measure the five parameters of the detector resolution function (three scale factors and two parameters giving the relative normalizations of the Gaussians) using $J/\psi \rightarrow \mu^+\mu^-$ candidates. These are selected using criteria similar to those for $D^*\pi$, except that both tracks are required to be identified as muons, and their invariant mass is required to be consistent with that of the J/ψ . Vertex positions are obtained independently for each track, in the same way as described above. The quantity $\Delta z = z_{\mu^+} - z_{\mu^-}$ then describes the detector resolution, which is the convolution of the two vertex resolutions, since for $J/\psi \rightarrow \mu^+\mu^-$ the underlying PDF is a delta function.

We perform an unbinned maximum likelihood fit using events in the J/ψ signal region in the di-muon invariant mass, and using sideband regions to determine the shape of the background under the peak. The underlying Δz PDF of the background is parametrized in the same way as that used for continuum, described above. Two sets of parameters are simultaneously determined for SVD1 and SVD2 data. We also take a possible offset into account, so that there are in total 16 free parameters in this fit (five describing the resolution function, two describing the background, and one Δz offset, each for SVD1 and SVD2 data). The result is shown in Fig. 7.

F. Background Δt Shape

The free parameters in the background PDFs P_{unco} and P_{corr} are determined using data from sideband regions. To measure the uncorrelated background shape, we use events in a side-band region of $-0.5 < \cos \delta_{\pi_f \pi_s} < 0.5$, which by definition is only populated by uncorrelated background, thus providing a very large sample to extract the various components of this background. We perform a simultaneous fit to OF and SF candidates, in both SVD1 and SVD2 data.

To obtain the correlated background parameters, a simultaneous fit is carried out to OF and SF events in a sideband region of $0.85 < \cos \delta_{\pi_f \pi_s} < 0.90$, $1.93 \text{ GeV}/c < p_{\pi_f} < 2.13 \text{ GeV}/c$ and $-1.7 < \cos \theta_{\text{hel}} < -0.3$. This sideband region is dominated by correlated and uncorrelated

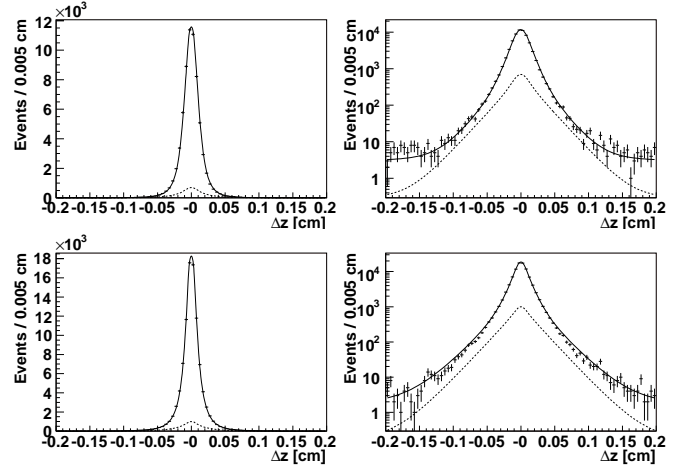


FIG. 7: Result of the resolution parameter extraction procedure for $J/\psi \rightarrow \mu^+\mu^-$ candidates selected from (top) SVD1 and (bottom) SVD2 data, shown with both (left) linear and (right) logarithmic coordinate scales. The data points show the Δz distribution for candidates in the signal region; the full line shows the result of the fit. The dashed line indicates the background.

backgrounds—the contributions from $D^*\pi$ and $D^*\rho$ are found to be small in MC. The uncorrelated background parameters are fixed to the values found in the previous fit, except the Δz offset (which are the same as that of correlated background) and the wrong-tag fractions, as mentioned above.

G. Fit Result

In order to test our fit procedure, we first constrain S^+ and S^- to be zero and perform a fit in which τ_{B^0} and Δm (as well as two wrong tag fractions and eight offsets) are free parameters. We obtain $\tau_{B^0} = 1.495 \pm 0.012 \text{ ps}$ and $\Delta m = 0.506 \pm 0.006 \text{ ps}^{-1}$, where the errors are statistical only. These values are compatible with the current world averages [19]. Reasonable agreement with the input values is also obtained in MC. Furthermore, fits to the MC with S^{\pm} floated give results consistent with zero, as expected.

To extract the CP violation parameters we fix τ_{B^0} and Δm at their world average values, and fit with S^+ , S^- , two wrong tag fractions and eight offsets as free parameters. We obtain $S^+ = 0.048 \pm 0.028$ and $S^- = 0.034 \pm 0.027$ where the errors are statistical only. The wrong tag fractions are $w_- = (4.8 \pm 1.6)\%$ and $w_+ = (3.4 \pm 1.6)\%$. All floating offsets are consistent with zero except the one for the $\pi^-\ell^+$ combinations in the SVD1 sample. The results are shown in Fig. 8. To further illustrate the CP violation effect, we define asymmetries in the same flavour events (\mathcal{A}^{SF}) and in the op-

posite flavour events (\mathcal{A}^{OF}), as

$$\begin{aligned}\mathcal{A}^{\text{SF}} &= \frac{N_{\pi^-l^-}(\Delta z) - N_{\pi^+l^+}(\Delta z)}{N_{\pi^-l^-}(\Delta z) + N_{\pi^+l^+}(\Delta z)}, \\ \mathcal{A}^{\text{OF}} &= \frac{N_{\pi^+l^-}(\Delta z) - N_{\pi^-l^+}(\Delta z)}{N_{\pi^+l^-}(\Delta z) + N_{\pi^-l^+}(\Delta z)},\end{aligned}\quad (15)$$

where the N values indicate the number of events for each combination of fast pion and tag lepton charge. These are shown in Fig. 9. Note that due to the relative contributions of the sine terms in Eq. 1, vertex biases (*i.e.* non-zero offsets) can induce an opposite flavour asymmetry, whereas the same flavour asymmetry is more robust.

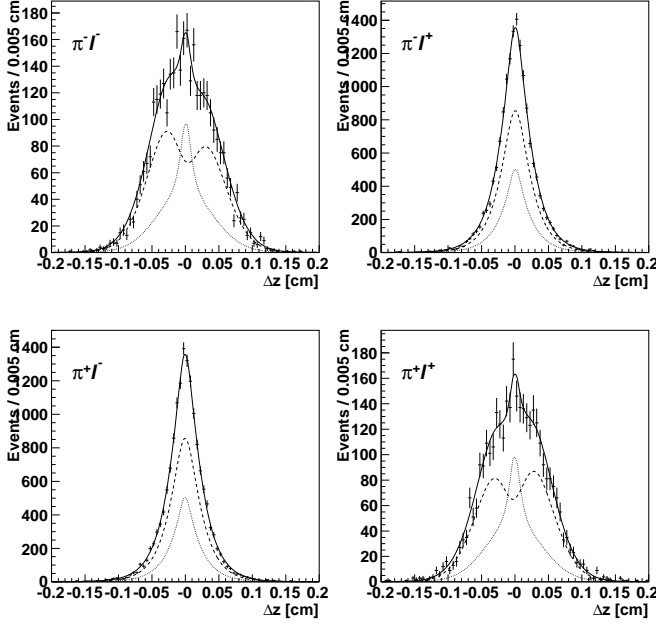


FIG. 8: Results of the fit to obtain S^+ and S^- . The fit result is superimposed on the data. The signal component is shown as the dashed line. The dotted line indicates the background contribution.

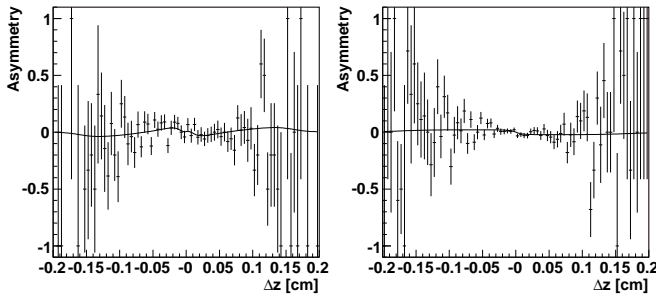


FIG. 9: Results of the fit to obtain S^+ and S^- , shown as asymmetries in the (left) same flavour events and (right) opposite flavour events. The fit result is superimposed on the data.

H. Systematic Error

Systematic errors due to the resolution function, the background fractions, the background parameters, and physics parameters are estimated by varying the values used in the fit by $\pm 1\sigma$. Systematic effects due to differences between data and MC in the distributions used in the kinematic fit are further investigated by repeating the fit using different binning. We repeat the entire fit procedure using twice as many bins in each of the three discriminating variables. Since $\cos \delta_{\pi_f \pi_s}$ is used in the best candidate selection, we also repeat the algorithm without using this variable in the kinematic fit. The largest deviation (0.007) is assigned as a systematic error.

The resolution function parameters are precisely determined from the fit to $J/\psi \rightarrow \mu^+ \mu^-$ candidates. We consider systematic effects due to our lack of knowledge of the exact functional form of the resolution function: using different parametrizations results in shifts of S^\pm as large as 0.008, which we assign as a systematic error. Allowing for effective S^\pm terms of ± 0.05 in the $D^* \rho$ and correlated background PDFs leads to systematic errors of 0.003 and 0.002, respectively.

Vertex biases may lead to a large systematic error on S^\pm , so we have introduced offsets to make our analysis relatively insensitive to such biases. These additional free parameters cause an increase in the statistical error of about 20%. In order to estimate the systematic error due to these offsets, we compare the results in MC simulations with and without the offsets. A difference of +0.011 is found for S^+ and is assigned as a systematic error for the offsets. We have further tested our fit routine for possible fit biases, such as could be caused by neglecting terms of $R_{D^* \pi}^2$ in the fit, by generating a number of large samples of signal MC with different input values of S^+ and S^- . All results come out consistent with the input values, without evidence of any bias.

The systematic errors are summarized in Table V. The total systematic error (0.017) is obtained by adding the above terms in quadrature.

TABLE V: Summary of the systematic errors in the S^\pm measurements using the partial reconstruction method.

Source	Error
Resolution fit	0.002
Resolution models	0.008
Kinematic smearing	0.002
Non-primary tracks	0.004
Background shapes	negligible
Kinematic fit	0.007
τ_{B^0} , Δm	0.001
CP violation in $D^* \rho$ and corr. bkgd.	0.004
Vertexing	0.011
Total	0.017

I. Result

The results using the partial reconstruction method are

$$\begin{aligned} S^+ &= 0.048 \pm 0.028 \pm 0.017, \\ S^- &= 0.034 \pm 0.027 \pm 0.017, \end{aligned} \quad (16)$$

where the first error is statistical and the second error is systematic.

V. DISCUSSION

A. Final results of $S^\pm(D^*\pi)$ and $S^\pm(D\pi)$

The $D^*\pi$ signal candidates in the full reconstruction sample and the partial reconstruction sample are mostly independent. We find only 60 $D^*\pi$ candidates which enter both samples. We repeat the analysis of the partial reconstruction sample after removing those overlapping candidates and obtain the same result. Therefore we combine the two results. Some part of the systematic errors in the two measurements may be correlated. We conservatively assume that contributions from physics parameters and fit biases (fit and MC bias in the full reconstruction sample and Δz offsets in the partial reconstruction sample) in the two measurements are 100% correlated, and combine them by taking a weighted average using the inverse of the statistical errors as weights. The final results are

$$\begin{aligned} S^+(D^*\pi) &= 0.049 \pm 0.020 \pm 0.011, \\ S^-(D^*\pi) &= 0.031 \pm 0.019 \pm 0.011, \\ S^+(D\pi) &= 0.031 \pm 0.030 \pm 0.012, \\ S^-(D\pi) &= 0.068 \pm 0.029 \pm 0.012 \end{aligned} \quad (17)$$

where the first errors are statistical and the second errors are systematic. These results are shown in Fig. 10 in terms of 1σ , 2σ and 3σ allowed regions in the S^- versus S^+ space. Small possible correlations in the systematic errors of S^+ and S^- are neglected.

The results for $D^*\pi$ and $D\pi$ decay modes show that the $(S^+ + S^-)$ values are 2.5σ and 2.2σ away from zero while the $(S^+ - S^-)$ values are within 1σ of zero. Since $(S^+ + S^-) \propto \sin(2\phi_1 + \phi_3) \cos \delta$ and $(S^+ - S^-) \propto \cos(2\phi_1 + \phi_3) \sin \delta$ (Eq. 2), it can be seen that these results are consistent with both $\delta_{D^*\pi}$ and $\delta_{D\pi}$ being small, as predicted by some theoretical models [5]. The significance of CP violation, seen as deviations of $(S^+ + S^-)$ from zero, is 2.5σ for $D^*\pi$ and 2.2σ for $D\pi$ decay modes.

B. Constraints on $(2\phi_1 + \phi_3)$ and R

Since we have two measurements (S^+ and S^-) which depend on three unknowns (R , $2\phi_1 + \phi_3$, δ), there is

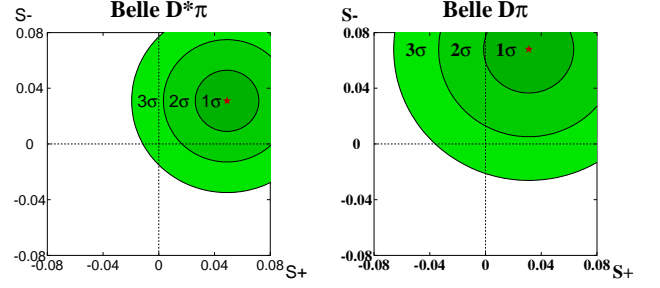


FIG. 10: Results of the S^\pm measurements expressed in terms of S^- vs S^+ for the $D^*\pi$ (left) and $D\pi$ (right) modes. Shaded regions indicate allowed regions with 1σ , 2σ and 3σ uncertainties defined by $\sqrt{-2\ln\mathcal{L}} = 1, 4, 9$, respectively

not sufficient information to solve for the weak phase $(2\phi_1 + \phi_3)$. Instead we obtain exclusion regions in two-dimensional space for any value of the third variable. The regions of $(2\phi_1 + \phi_3, R)$ space that are excluded at the $1, 2, 3\sigma$ levels are shown in Fig. 11. An alternative representation, shown in Fig. 12, gives the lower bound on $|\sin(2\phi_1 + \phi_3)|$ for any values of R and δ .

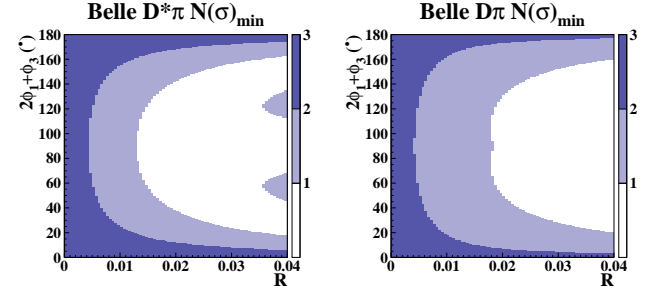


FIG. 11: Excluded regions of $(2\phi_1 + \phi_3)$ vs R space at $1, 2, 3\sigma$ level for the $D^*\pi$ (left) and $D\pi$ (right) decays. The range $0^\circ - 180^\circ$ for $2\phi_1 + \phi_3$ is shown; there are additional solutions at $2\phi_1 + \phi_3 \rightarrow 2\phi_1 + \phi_3 + 180^\circ$.

Further conclusions cannot be drawn without some theoretical estimate of the values of either $R_{D^{(*)}\pi}$ or $\delta_{D^{(*)}\pi}$. One interesting possibility is to estimate the size of $R_{D^{(*)}\pi}^2$ using decays such as $B^+ \rightarrow D^{(*)}\pi^0$ and $B^0 \rightarrow D_s^{(*)\pm}\pi^\mp$, which are related to $B^0 \rightarrow D^{(*)}\pi^\mp$ by isospin and $SU(3)$, respectively [2].

The method using $SU(3)$ symmetry has some experimental advantages, since the rates are enhanced by the square of the tangent of the Cabibbo angle θ_c . The relevant expression is

$$R_{D^{(*)}\pi}^2 = \tan^2 \theta_c \left(\frac{f_{D^{(*)}}}{f_{D_s^{(*)}}} \right)^2 \frac{\mathcal{B}(B^0 \rightarrow D_s^{(*)+}\pi^-)}{\mathcal{B}(B^0 \rightarrow D^{(*)-}\pi^+)}, \quad (18)$$

where f_M is the decay constant for the M -meson. The equality is valid up to $SU(3)$ breaking effects. Both

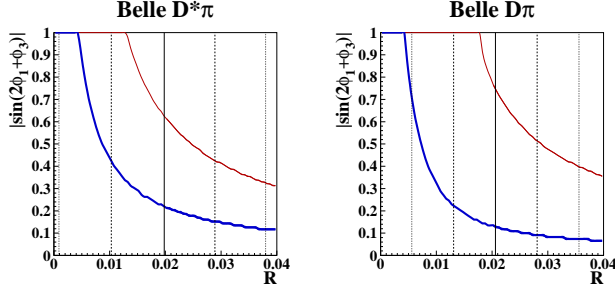


FIG. 12: Lower limit on $|\sin(2\phi_1 + \phi_3)|$ as a function of R at 1σ (68% CL) (thick curves) and 2σ (95% CL) (thin curves) from (left) $D^*\pi$ and (right) $D\pi$. The estimated values for $R_{D^{(*)}\pi}$ are indicated as solid lines (central values). Coarse dotted lines and fine dotted lines indicate their 1σ and 2σ errors.

Belle [26] and BaBar [27] have reported evidence for the decay $B^0 \rightarrow D_s^{*+}\pi^-$. BaBar included a limit for the $B^0 \rightarrow D_s^{*+}\pi^-$ mode in the same paper. We estimate $R_{D^*\pi}$ and $R_{D\pi}$ using the measured branching fractions and the form factors from a lattice QCD calculation by the UKQCD collaboration [28]. We use $\mathcal{B}(B^0 \rightarrow D_s^{*+}\pi^-)/\mathcal{B}(B^0 \rightarrow D^{*-}\pi^+) = 0.0068^{+0.0047}_{-0.0051}$, which is determined from the BaBar result $\mathcal{B}(B^0 \rightarrow D_s^{*+}\pi^-) = (1.9^{+1.2}_{-1.3} \pm 0.5) \times 10^{-5}$ and the PDG 2004 value $\mathcal{B}(B^0 \rightarrow D^{*-}\pi^+) = (2.76 \pm 0.21) \times 10^{-3}$, and $\mathcal{B}(B^0 \rightarrow D_s^{*+}\pi^-)/\mathcal{B}(B^0 \rightarrow D^-\pi^+) = 0.0098 \pm 0.0040$, which is determined from the PDG 2004 values of $\mathcal{B}(B^0 \rightarrow D_s^{*+}\pi^-) = (2.7 \pm 1.0) \times 10^{-5}$ and $\mathcal{B}(B^0 \rightarrow D^-\pi^+) = (2.76 \pm 0.25) \times 10^{-3}$. The decay constant ratios are $f_{D^*}/f_{D_s^*} = 1.04 \pm 0.01 \pm 0.02$ and $f_D/f_{D_s} = 0.90 \pm 0.01 \pm 0.01$. We use $\tan\theta_c = 0.23$ [19, 29].

Adding $\pm 30\%$ theory uncertainty for SU(3) breaking effects, such as contributions from annihilation diagrams, we obtain

$$\begin{aligned} R_{D^*\pi} &= 0.020 \pm 0.007 \pm 0.006(\text{theory}), \\ R_{D\pi} &= 0.021 \pm 0.004 \pm 0.006(\text{theory}) \end{aligned} \quad (19)$$

as indicated in Fig. 12. If we use these values, we can restrict the allowed region of $|\sin(2\phi_1 + \phi_3)|$ to be

$$|\sin(2\phi_1 + \phi_3)| > 0.44 \text{ (0.13) at } 68\%(95\%) \text{ CL} \quad (20)$$

from the results for the $D^*\pi$ mode and

$$|\sin(2\phi_1 + \phi_3)| > 0.52 \text{ (0.07) at } 68\%(95\%) \text{ CL} \quad (21)$$

from the results for the $D\pi$ mode, respectively.

VI. SUMMARY

We have measured CP violation parameters that depend on ϕ_3 using the time-dependent decay rates of the

$B^0 \rightarrow D^{(*)\mp}\pi^\pm$. A total of 386 million $B\bar{B}$ events were used in the analysis. While the $D\pi$ sample was collected by a standard full reconstruction method, the $D^*\pi$ sample was enlarged by using, in addition, a partial reconstruction technique, essentially doubling the statistical power of this mode.

The final results expressed in terms of S^+ and S^- , which are related to the CKM angles ϕ_1 and ϕ_3 , the ratio of suppressed to favoured amplitudes, and the strong phase difference between them, as $S^\pm = -R_{D^*\pi} \sin(2\phi_1 + \phi_3 \pm \delta_{D^*\pi}) / (1 + R_{D^*\pi}^2)$ for $D^*\pi$ and $S^\pm = +R_{D\pi} \sin(2\phi_1 + \phi_3 \pm \delta_{D\pi}) / (1 + R_{D\pi}^2)$ for $D\pi$, are

$$\begin{aligned} S^+(D^*\pi) &= 0.049 \pm 0.020 \pm 0.011, \\ S^-(D^*\pi) &= 0.031 \pm 0.019 \pm 0.011, \\ S^+(D\pi) &= 0.031 \pm 0.030 \pm 0.012, \\ S^-(D\pi) &= 0.068 \pm 0.029 \pm 0.012, \end{aligned} \quad (22)$$

where the first errors are statistical and the second errors are systematic. These results are an indication of CP violation in $B^0 \rightarrow D^{*-}\pi^+$ and $B^0 \rightarrow D^-\pi^+$ decays at the 2.5σ and 2.2σ levels, respectively. If we use the values of $R_{D^*\pi}$ and $R_{D\pi}$ that are determined using a combination of factorization and SU(3) symmetry assumptions, the branching fraction measurements for the $D_s^{(*)}\pi$ modes, and lattice QCD calculations, we obtain 68% (95%) confidence level lower limits on $|\sin(2\phi_1 + \phi_3)|$ of 0.44 (0.13) and 0.52 (0.07) from the $D^*\pi$ and $D\pi$ modes, respectively.

Acknowledgements

We thank the KEKB group for the excellent operation of the accelerator, the KEK cryogenics group for the efficient operation of the solenoid, and the KEK computer group and the National Institute of Informatics for valuable computing and Super-SINET network support. We acknowledge support from the Ministry of Education, Culture, Sports, Science, and Technology of Japan and the Japan Society for the Promotion of Science; the Australian Research Council and the Australian Department of Education, Science and Training; the National Science Foundation of China under contract No. 10175071; the Department of Science and Technology of India; the BK21 program of the Ministry of Education of Korea and the CHEP SRC program of the Korea Science and Engineering Foundation; the Polish State Committee for Scientific Research under contract No. 2P03B 01324; the Ministry of Science and Technology of the Russian Federation; the Ministry of Higher Education, Science and Technology of the Republic of Slovenia; the Swiss National Science Foundation; the National Science Council and the Ministry of Education of Taiwan; and the U.S. Department of Energy.

-
- [1] M. Kobayashi and T. Maskawa, *Prog. Theor. Phys.* **49** 652 (1973).
 - [2] I. Dunietz and R.G. Sachs, *Phys. Rev. D* **37** 3186 (1988), *Erratum: Phys. Rev. D* **39** 3515 (1989); I. Dunietz, *Phys. Lett. B* **427** 179 (1998).
 - [3] R. Fleischer, *Nucl. Phys. B* **671** 459 (2003).
 - [4] D.A. Suprun, C.-W. Chiang and J.L. Rosner, *Phys. Rev. D* **65** 054025 (2002).
 - [5] L. Wolfenstein, *Phys. Rev. D* **69** 016006 (2004).
 - [6] Y. Zheng, T.E. Browder *et al.*, *Phys. Rev. D* **67**, 092004 (2003).
 - [7] T. Sarangi, K. Abe *et al.*, *Phys. Rev. Lett.* **93**, 031802 (2004).
 - [8] T. Gershon *et al.*, *Phys. Lett. B* **624**, 11 (2005).
 - [9] B. Aubert *et al.*, *Phys. Rev. Lett* **92**, 251802 (2004).
 - [10] B. Aubert *et al.*, *Phys. Rev. D* **71**, 112003 (2005).
 - [11] A. Abashian *et al.* (Belle Collaboration), *Nucl. Instr. and Meth. A* **479**, 117 (2002).
 - [12] S. Kurokawa, *Nucl. Instr. and Meth. A* **499**,1 (2003).
 - [13] Y. Ushiroda, *Nucl. Instr. and Meth. A* **511**, 6 (2003).
 - [14] K. Abe *et al.* (Belle Collaboration), *Phys. Rev. D* **66**, 032007 (2002).
 - [15] K. Abe *et al.* (Belle Collaboration), *Phys. Rev. D* **71**, 072003 (2005).
 - [16] H. Albrecht *et al.* (ARGUS Collaboration), *Phys. Lett. B* **241**, 278 (1990).
 - [17] K. Abe *et al.* (Belle Collaboration), *Phys. Rev. Lett.* **88**, 171801 (2002).
 - [18] O. Long, M. Baak, R.N. Cahn and D. Kirkby, *Phys. Rev. D* **68** (2003) 034010.
 - [19] S. Eidelman *et al.* (Particle Data Group), *Phys. Lett. B* **592**,1 (2004).
 - [20] G.C. Fox and S. Wolfram, *Phys. Rev. Lett.* **41** 1581 (1978).
 - [21] Branching fractions for $B \rightarrow D^{**}\pi$ decays, which dominate the correlated background, are estimated based on K. Abe *et al.*, *Phys. Rev. D* **69**, 112002 (2004) and K. Abe *et al.*, BELLE-CONF-0460, hep-ex/0412072.
 - [22] N. Sinha and R. Sinha, *Phys. Rev. Lett.* **80**, 3706 (1998), D. London, N. Sinha and R. Sinha, *Phys. Rev. Lett.* **85**, 1807 (2000).
 - [23] H. Tajima *et al.*, *Nucl. Instr. and Meth. Phys. Res., Sect. A* **533**, 370 (2004).
 - [24] A small amount of data is reprocessed using a set of constants which is corrected for the small relative misalignment of the SVD and CDC. The correction function is calculated from comparisons of the vertex positions for tracks between the two reprocessings.
 - [25] F. Ronga, Thèse de Doctorat, Université de Lausanne (2003).
 - [26] P. Krokovny *et al.*, *Phys. Rev. Lett.* **89**, 231804 (2002).
 - [27] B. Aubert *et al.*, *Phys. Rev. Lett.* **90**, 181803 (2003).
 - [28] K.C. Bowler *et al.*, *Nucl. Phys. B* **619**, 507 (2001).
 - [29] E. Blucher *et al.*, hep-ph/0512039.